

Investigation on three-dimensional marine dune modelling validation

Nicolas Michelet¹, Fabien Leckler¹, Maëlle Nexer¹, Noémie Durand¹, and Alice Lefebvre²

¹France Energies Marines

²MARUM - University of Bremen

November 8, 2023

Abstract

The comparison of a morphodynamic model results with observations is an essential part to establish its credibility. In the past multiple model were validated against observations for sand banks, coastlines or estuarine environments. Some modelling have studied the marine dunes migrations but are generally limited to a two-dimensional study. In the present study, a three-dimensional morphodynamic model were setup on an area where highly dynamic dunes are present. The modelling results were analysed and compared to in-situ observations either using a 2D and a 3D method. The vertical and horizontal differences with observations were then assessed using the known method and, based on these results, an updated validation method were proposed to overcome some issues that could interfere with the process.

Hosted file

977546_0_art_file_11544268_s3vfhl.docx available at <https://authorea.com/users/695870/articles/684374-investigation-on-three-dimensional-marine-dune-modelling-validation>

1 **Investigation on three-dimensional marine dune modelling validation**

2

3 **Nicolas Michelet¹, Fabien Leckler¹, Maelle Nexer¹, Noémie Durand¹ and Alice Lefebvre²**

4

5 ¹France Energies Marines, 525 Avenue Alexis de Rochon, 29280 Plouzané, France.

6

²Marum – Center for Marine environment Sciences, University of Bremen, Germany.

7

8 Corresponding author: Nicolas Michelet (nicolas.michelet@france-energies-marines.org)

9

10 **Key Points:**

11

- Marine dune

12

- Morphodynamic model

13

- Validation method

14

15 Abstract

16 The comparison of a morphodynamic model results with observations is an essential part to
17 establish its credibility. In the past multiple models were validated against observations for sand
18 banks, coastlines or estuarine environments. Some models have studied the marine dunes
19 migrations but are generally limited to a two-dimensional study. In the present study, a three-
20 dimensional morphodynamic model was setup on an area where highly dynamic dunes are
21 present. The modelling results were analysed and compared to *in-situ* observations either using a
22 2D or a 3D method. The vertical and horizontal differences with observations were then assessed
23 using the known method and, based on these results, an updated validation method were
24 proposed to overcome some issues that could interfere with the process.

25

26 Plain Language Summary

27 To assess the reliability of a model, an essential part is to compare the results with field
28 measurements. In the past, multiple models were setup up on sand banks, coastlines or estuarine
29 environments and takes credibility with this kind of comparisons. Studies of the marine dune
30 migration is generally made along two dimensions: the migration direction and the water depth.
31 In the present study, a model is setup on a marine environment and accounts for three-
32 dimensions to analyze the dunes' evolution over an area. The model validity is assessed using the
33 known method and based on these results, an updated validation method was proposed to
34 overcome some issues that could interfere with the process.

35

36 1 Introduction

37 The development of marine renewable energy has become a priority for many countries as part
38 of the solution to limit the impacts of climate change while considering the global growing need
39 in electricity. In the European Union, the offshore wind industry aims for an installed capacity of
40 300 GW by 2050. This will surely induce the multiplication of infrastructures in the North Sea
41 and the English Channel as it accounts for a large part of the energy potential. These shallow
42 seas are however covered by active bedforms (Le Bot & Trentesaux, 2004 ; Damen et al., 2018)
43 with heights that can reach 20-25 % of the water depth (Knaapen et al., 2001; Damen et al.,
44 2018) and migration speeds up to tens of meters per year (Blondeaux and Vittori, 2016). Given
45 these characteristics, these bedforms, also called marine dunes, are likely to pose specific
46 challenges for the offshore windfarm industry. Their migration could induce scouring issues
47 around the foundations or expose the buried cables over time increasing the risk of damage
48 (Whitehouse et al., 2000 ; Barrie and Conway, 2014).

49 To understand the impact of marines dunes on offshore structures and vice versa, numerical
50 modelling appears as one solution. Multiple numerical process-based models were developed to
51 investigate marine dune migration, height and shape evolution over time and the processes that
52 affect them (Németh et al., 2007 ; Van den Berg et al., 2012 ; Doré et al., 2018). However, most
53 of these studies are focused on dune development starting from a flat bed which limits their
54 applicability to study the long term evolution of marine dune fields. Tonnon et al. (2007) and
55 Krabbendam et al. (2021) were the first to model dune dynamics over multiple years starting
56 with an initial realistic bathymetry. They assessed the capability of the model to reproduce the
57 evolution of large bedforms over a decade. For this, they used a two-dimensional vertical (2DV)

58 numerical model. The results were compared to the evolution of a dune field along a bathymetric
59 transect extracted perpendicular to the crestlines. In areas where dunes are mostly rectilinear, it is
60 reasonable to assume that most variations will be captured by a transect. However, most marine
61 dune fields exhibit at least some degree of three-dimensionality which would not be well
62 represented using a 2D model. The use of a three-dimensional (3D) model seems thus necessary.
63 However, how a morphodynamic model can be validated specifically to assess its ability to
64 reproduce marine dune evolution is not yet established.

65 To validate a morphodynamic model over a shallow water area, the Brier Skill Score (BSS) is
66 often used (Sutherland et al., 2004, Luijendijk et al., 2017). This single-number metric allows to
67 assess the relative accuracy of morphodynamic simulations based on height difference between
68 final observed and modelled states weighted with an initial state (Sutherland et al., 2004). This
69 skill score has been used for modelling of coastlines (Luijendijk et al., 2017 ; Bennet et al.,
70 2019), sand banks and bar movement (Sutherland et al., 2004) or even estuarine evolution (Scott
71 and Mason, 2007 ; Dam et al., 2016). However, these studies mainly focus on coastal areas
72 where the water depth is the key variable to assess the reliability of the models. For bedforms
73 migrations, the water depth is also an important aspect but the use of only the BSS on the water
74 depth might not be sufficient for the validation process. For example, Sutherland et al. (2007)
75 have described a sand bar migration to illustrate the application of the BSS. The modelling of the
76 outer bar depth shows a good agreement, while a significant error is estimated on the crest
77 position. In their study it represents only one crest and does not impact the results. However, on
78 other areas, differences on the crest positions could induce a misrepresentation of the sediment
79 flux and bring errors on the long-term simulation. The crest positions might then need to be
80 considered in the validation process.

81 The present study addresses the question of the validation of a morphodynamic model focused
82 on the estimation of marine dune migration. The study area, off the Dunkirk coast, is described
83 in section 2.1. The numerical systems, the Coastal and Regional Ocean COmmunity (CROCO)
84 (Auclair et al., 2022) coupled with the USGS sediment module (Blaas et al., 2007 ; Warner et
85 al., 2008) and their setup, in the eastern part of the English Channel and the southern part of the
86 North Sea, are described in section 2.2 and section 2.3. The validation of the hydrodynamic
87 predictions were assessed against in-situ measurements (section 3.1). Morphodynamic results,
88 were studied either following a two-dimensional (section 3.2) and a three-dimensional (3D)
89 (section 3.3) method before the proposal of a 3D validation of the modelling of the migration of
90 marine dunes (section 3.4). All results are finally discussed in section 4.

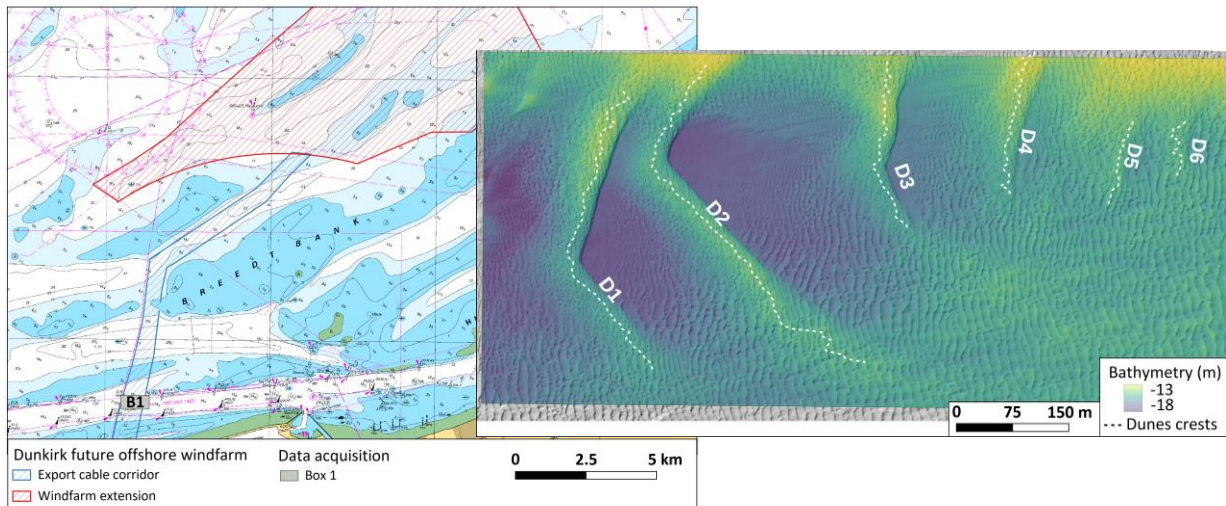
91

92 **2 Data and method**

93 2.1 Study site

94 The site of application is located off the Dunkirk coasts in the southern part of the North Sea, a
95 few kilometers east of the Dover Strait (Figure 1, left) in France. In this area the hydrodynamics
96 are dominated by the tidal currents with a typical mean spring tidal range of 5.5 m at the Dunkirk
97 tide gauge.

98



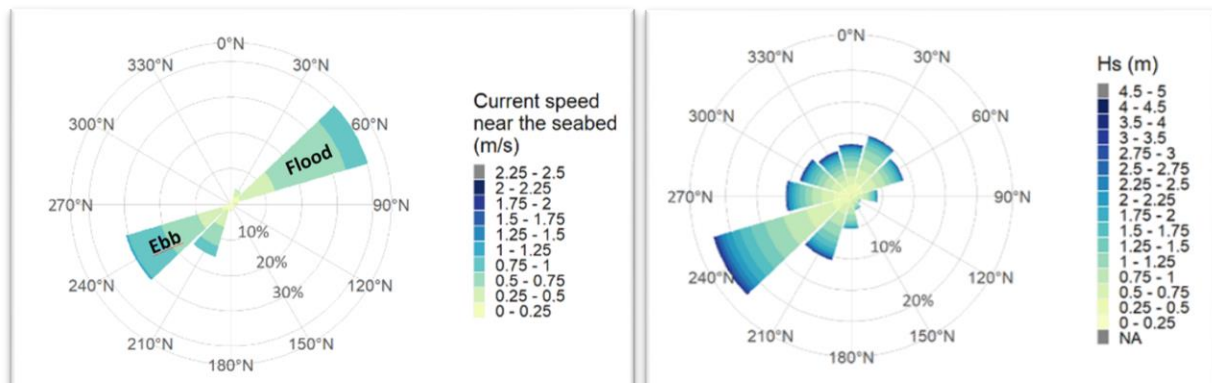
99

100 **Figure 1. (left) Location of Dunkirk windfarm area (in red) and the area of interest where**
 101 **bathymetric surveys were performed noted B1 on the figure. (right) Bathymetric data of**
 102 **B1 area collected on the first survey of the 17 November 2019. All six dunes are numbered**
 103 **on the figure (D1-D6) and their crestlines are represented by the white dash-lines.**

104

105 In this area, the tidal wave is considered progressive (Bonnetille et al., 1971). As a result, the
 106 maximum flood and ebb current magnitude happen at the time of, respectively, the high and low
 107 water level. The flood component, trending north-east with current amplitude up to 1.25 m/s, is
 108 generally stronger than the ebb which is directed toward the south-west with current amplitude
 109 up to 0.75 m/s (Figure 2, left). Regarding the waves, a major direction of origins was identified
 110 with the measurements of the Westhinder lightboat. Waves principally comes from the English
 111 Channel in the south-west while the rest comes from the inner basin of the North Sea in the
 112 north-west and north-east. Still according to the measurements, waves height range from 1 to 3
 113 m and their periods are between 4 and 10 s (Figure 2, right).

114



115 **Figure 2. (left) Current speed near the seabed rose based on ADCP measurement (Nexer et**
 116 **al., 2023). (right) Offshore wave rose at Westhinder lightboat (51°22'51" N – 2°26'08" E)**
 117 **(Source data: Flanders Marine Institute).**

118

119 This study focuses on a domain referred to as B1 (Figure 1, right), located along the future
 120 windfarm export cable corridor (Figure 1, left). Over this B1 area, 8 bathymetric surveys and
 121 multiple sediment samplings were performed between November 2019 and July 2021. In this
 122 study the bathymetry is expressed as the water depth with respect to the mean sea level (MSL).
 123 With a bathymetry ranging from 15 to 20 m, the area is composed of six very large dunes named
 124 D1-D6 with, from west to east, two barchans, a sinuous and three rectilinear dunes (Figure 1,
 125 right). The bathymetric data were analyzed in a preliminary study where a low-pass filter was
 126 applied to remove most secondary bedforms. The filtering is intentionally kept light to avoid too
 127 much modification of the primary dunes. Crests and troughs were identified manually
 128 respectively as the lowest and highest bathymetry point along longitudinal profiles (Nexer et al.,
 129 2023). According to these results, dune height and crestline length are decreasing from west to
 130 east (Table 1). The two barchans D1 and D2 are the largest dunes with respectively average
 131 height of 2.12 and 2.03 m and crestline length of 509.8 m and 599.52 m. Except for dune D4, the
 132 width (distance between the two dune troughs), follow the same schema with a value decreasing
 133 from west to east. The presence of the two barchans suggests that there is either a strong lateral
 134 variability of the sediment type (Ernsten et al., 2004) or a lack of sediment (Belderson et al.,
 135 1982). Bed samples showed that the seabed is uniformly composed of medium sand with $d_{50} =$
 136 $327.78 \mu\text{m}$ and $d_{90} = 557.62 \mu\text{m}$. Therefore, there is some indication that the environment may
 137 be sediment-starved.

138

139 **Table 1. Heights, lengths and crestline lengths of all six dunes of B1 area measured on**
 140 **November the 17th 2019 (Nexer et al., 2023).**

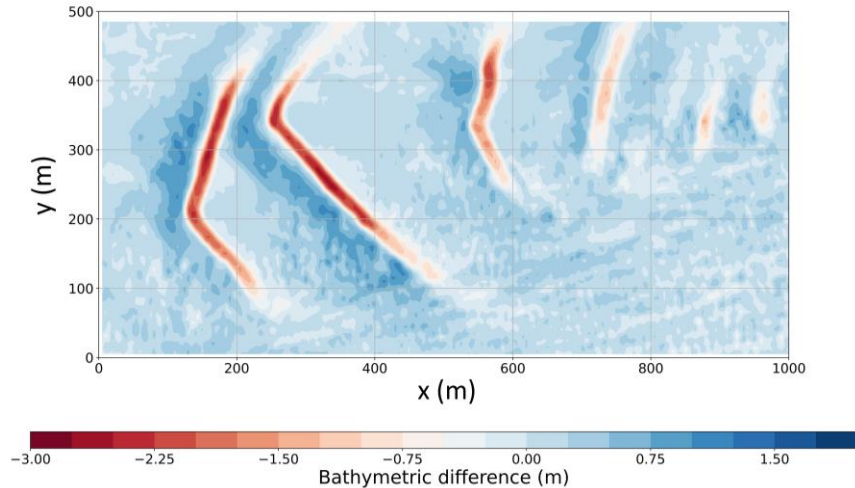
141

Dune name	Dune 1	Dune 2	Dune 3	Dune 4	Dune 5	Dune 6
Height (m)	2.12	2.03	1.64	1.16	0.92	0.78
Width (m)	140	140	135	152	132	66
Crestline length (m)	510	600	290	230	124	100

142

143 The comparison between the different surveys shows that the area is highly dynamic with a
 144 migration directed to the east at an average rate of 28.5 m/year with high variations between the
 145 different periods (Nexer et al., 2023). This eastern migration is explained by the influence of the
 146 asymmetrical tidal flow (Nexer et al., 2023). In this study, the 4 months period between the first
 147 2 surveys (S1 on 17 November 2019 and S2 on 18 March 2020) are considered. During this
 148 period the dunes were highly dynamic with a migration rate ranging from 53.4 to 64.4 m/year.
 149 Figure 3 represents the bathymetric difference between these observations. Over the locations of
 150 each dune, eastward migration can be recognised as a positive difference on the western part of
 151 each dunes and a negative difference on the eastern part. Height differences up to 2.5 m are
 152 observed around the middle of the first two dunes while these changes decrease to 1.8 m on the
 153 northern part of Dune 3 and around 1 m for the other three dunes. These results imply that during
 154 these 4 months, the crests have moved toward the east and are standing on the initial eastern
 155 troughs positions. During the study period, the general migration schema can then be
 156 summarized as a movement of each dunes through the east with no significant changes of their
 157 horizontal shapes.

158



159
160

161 **Figure 3. Bathymetric difference between final (S2) (18/03/2020) and initial (S1)**
162 **(17/11/2019) observations.**

163

2.2 Models description

164 CROCO is a three-dimensional, free-surface numerical model that solves finite-difference
165 approximation of the Reynolds-Averaged Navier Stokes (RANS) equation using the hydrostatic
166 and Boussinesq approximations. The computation is performed using a C-Arakawa grid over
167 horizontal dimensions and a terrain-following σ coordinate along the vertical dimension. The set
168 of equations is finally resolved using the mode-splitting technique that separates the barotropic
169 and baroclinic modes.

170 The morphodynamic is modelled using the USGS sediment model. The sediment is represented
171 as a constant number of layers that extend under the horizontal water cells (Warner et al., 2008).
172 Each layer is initialized with a thickness, sediment-class distribution, porosity and age. To
173 account for erosion and deposition, the active bed layer thickness evolves in time depending on
174 the transport. Here only the bedload transport is considered following the Wu & Lin (2014)
175 formulation which calculate the net transport rate as the sum of offshore and onshore bed-load
176 transport rate. The bed evolution is calculated using the Exner equation considering only bedload
177 transport.

178

2.3. Hydrodynamic setup

179 The computational domain has a 5 m horizontal resolution and covers the entire B1 area. The
180 flow is assumed to be turbulent over a rough bottom, characterized by the roughness parameter
181 z_0 defined as the height above the seabed at which the fluid velocity is zero. This parameter is
182 defined as constant over the area of modelling. It was set to 0.4 and 4 mm in the two
183 configurations considered in this study, referred to as C1 and C2. The calculation was performed
184 with a baroclinic timestep of $\Delta t_{3d} = 1$ s and a barotropic timestep of $\Delta t_{2D} = 1/12$ s. Initial
185 bathymetry is based on the initial survey performed on 17 November 2019 that were filtered as
186 described before. C1 and C2 configurations have been performed using boundary conditions
187 extracted from results coming from regional simulations using CROCO and WAVEWATCHIII®
188 (WW3) models. Both were setup to downscale from a large-scale domain to the same grid,

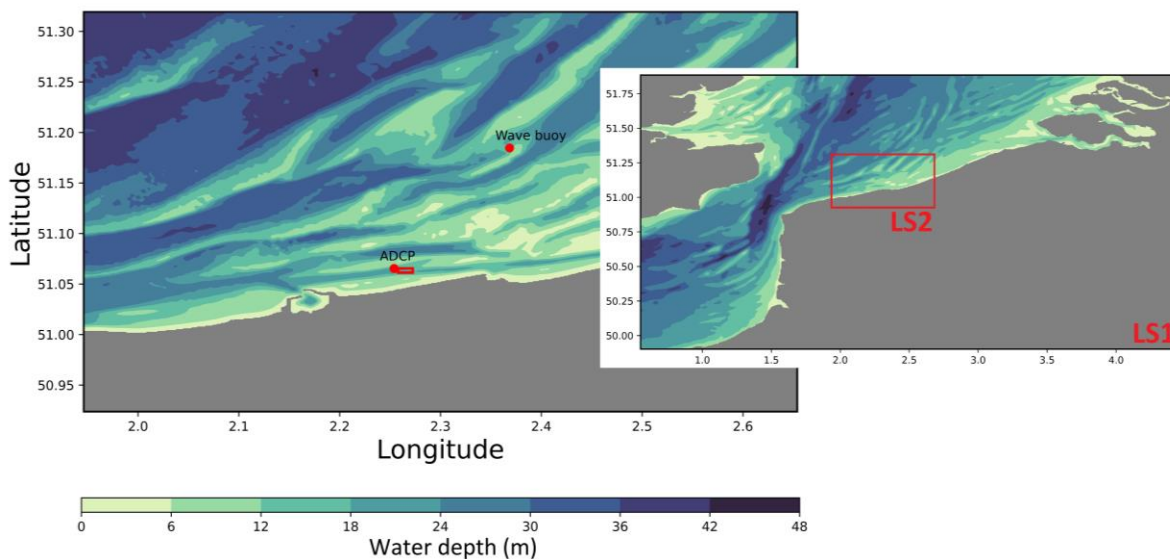
189 named LS2, that cover the future windfarm area of Dunkirk and the cable corridor with a spatial
 190 resolution of 100 m (Figure 4).
 191

192 **CROCO**

193 CROCO model downscale from a numerical domain that covers the eastern part of the English
 194 Channel and the southern part of the North Sea, called LS1 to LS2 domains (Figure 4). For both
 195 configurations, wind conditions were set using the AROME database. Boundary conditions of
 196 free-surface elevation and meridional and zonal component of the current were extracted from
 197 the MARC database (MARS3D configurations covering the French coasts and run operationally
 198 by Ifremer). The LS2 configuration considers LS1 results as boundaries. Along the water
 199 column, CROCO grid is configured using a total of 32 layers.
 200

201 **WAVEWATCHIII[®]**

202 The wave model WAVEWATCHIII[®] (WW3) is based on nested runs that are implemented to
 203 downscale from global scale to fine resolution grids. First, the global-scale simulation is obtained
 204 using a regular computational grid with a 0.5-degree spatial resolution forced with ERA5 wind
 205 fields. Then, an unstructured mesh, called NORGAS developed by Shom and run operationally
 206 for the French marine surge monitoring is used. NORGAS's mesh refines from 10 km resolution
 207 at the open deep-water boundaries to 250 m resolution at the coast. The mesh covers the Gulf of
 208 Biscay, the English Channel and the south of the North Sea and benefits from an accurate
 209 bathymetry. The wave model is forced with currents and water levels obtained from the 2 km-
 210 resolution ATLNE model of the MARC database. Wind forcing using ERA5 hindcast is
 211 consistently used. On the computational grid LS2, the model is forced at the open boundaries
 212 with the wave spectra obtained with the NORGAS mesh and current and water levels from
 213 CROCO regional run LS1. Consistently with ocean model, the high-resolution wave model grid
 214 is forced with AROME database.
 215
 216



217
 218
 219 **Figure 4. (left) Boundaries of the regional domain LS2. The locations of the ADCP and the**
 220 **wave buoy used for hydrodynamic validation are defined by the red dots. Area B1 is**
 221 **represented by the red box. (right) Boundaries of the regional domain LS1. The red box**

222 **represents the extension of the LS2 domain. Both color scales show the spatial distribution**
 223 **of the mean water depth, with respect to the mean sea level.**

224 2.3. Morphodynamic setup

225 In-situ analysis showed that the sediment is homogeneous over the area. Hence, a class of
 226 medium sand with $d_{50} = 328 \mu\text{m}$ is considered in the distribution. As reported before, the
 227 presence of barchans suggest that this area is sediment-starved. Since sampling performed either
 228 on the crests and troughs shows similar type of sediment (Nexer et al., 2023), considering the
 229 size of the dunes, a 3-m thick active layer is defined in this configuration which leaves enough
 230 amplitude to model the observed bathymetric differences (Figure 3). The porosity is set constant
 231 to 0.41 based on the analysis of the in-situ samples. Since no suspended sediment is considered,
 232 the sediment age is left to 0 the default value.

233 2.4. Outputs analysis

234 Hydrodynamic and morphodynamic results were assessed using the Root Mean Square Error
 235 (RMSE):

236

$$RMSE = \sqrt{\frac{\sum_{i=1}^N (X_{mod,i} - X_{obs,i})^2}{N}}$$

237

238 where X_{mod} and X_{obs} are respectively the predicted and observed variable and N the number of
 239 compared values. The hydrodynamic results were also evaluated using the index of agreement
 240 described by Willmott (1981) as:

241

$$RE = 1 - \frac{\sum_{i=1}^N (X_{obs,i} - X_{mod,i})^2}{\sum_{i=1}^N (|X_{mod,i} - \overline{X_{obs}}| + |X_{obs,i} - \overline{X_{obs}}|)^2}$$

242

243 where the overbar $\overline{X_{obs}}$ is the averaged of the observation. The index of agreement ranges from 0
 244 to 1 which described a perfect modelling.

245 The wave model performance was evaluated by comparing the significant wave height, mean
 246 direction and mean wave period T_{01} . The comparison is focused on T_{01} for its low order which
 247 gives more weight to the energetic waves, which are more important for sediment transport, than
 248 another type of period.

249 The morphodynamic analysis was based on the Brier Skill Score (BSS) (Sutherland et al., 2004)
 250 which is described as follow:

251

$$BSS = 1 - \frac{\langle (z_{mod} - z_{obs})^2 \rangle}{\langle (z_{ini} - z_{obs})^2 \rangle}$$

252

253

254 where z_{ini} is the initial bed level (here survey made the 17 November 2019), z_{obs} the final
 255 observation (here survey made the 18 March 2020) and z_{mod} the modelled bed level which is
 256 extracted on the same date as the final observation. The angular brackets $\langle \cdot \rangle$ denote the mean

257 over the area of interest. The BSS was also decomposed following the Murphy-Epstein
 258 decomposition (Murphy and Epstein, 1989) as follow:

259

$$BSS = \frac{\alpha - \beta - \gamma + \varepsilon}{1 + \varepsilon}$$

260

261 where α is the phase error which described the error in position. Perfect modelling of the phase
 262 gives $\alpha=1$. β is the amplitude error which described the error in terms of sediment volume
 263 displacement with perfect modelling with $\beta=0$. γ is the averaged bed level error with perfect
 264 modelling with $\gamma=0$. And to finish the ε represent the normalization term which is only affected
 265 by the measured changes from the baseline prediction (Sutherland et al., 2004).

266

$$\alpha = r_{\Delta_{mod}, \Delta_{obs}}^2 \quad \beta = \left(r_{\Delta_{mod}, \Delta_{obs}} - \frac{\sigma_{\Delta_{mod}}}{\sigma_{\Delta_{obs}}} \right)^2$$

267

$$\gamma = \left(\frac{\langle \Delta_{mod} \rangle - \langle \Delta_{obs} \rangle}{\sigma_{\Delta_{obs}}} \right)^2 \quad \varepsilon = \left(\frac{\langle \Delta_{obs} \rangle}{\sigma_{\Delta_{obs}}} \right)^2$$

268

269 with $r_{\Delta_{mod}, \Delta_{obs}} = \frac{\langle \Delta_{mod} \Delta_{obs} \rangle}{\sigma_{\Delta_{mod}} \sigma_{\Delta_{obs}}}$, $\Delta_{mod} = z_{mod} - z_{ini}$ and $\Delta_{obs} = z_{obs} - z_{ini}$.

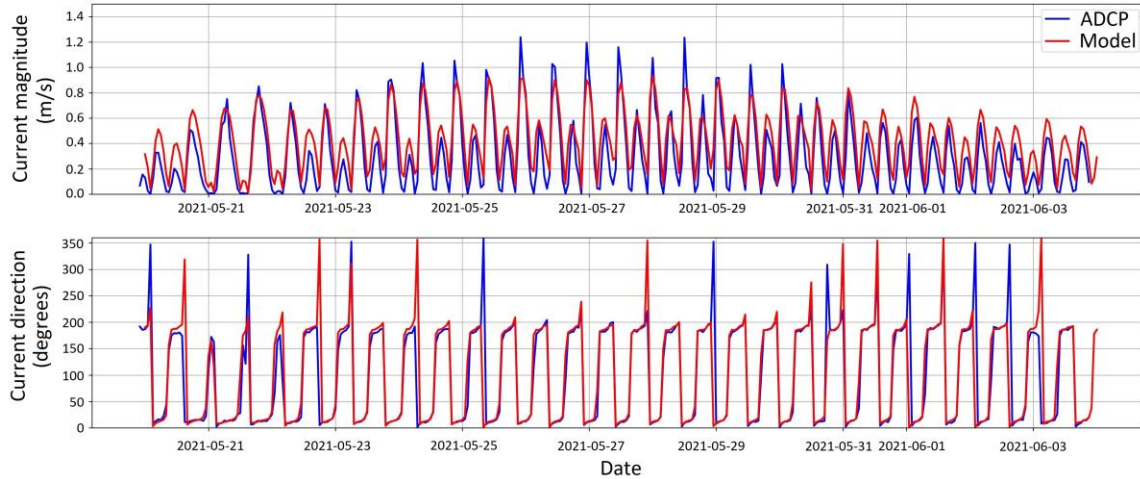
270 3 Results

271 3.1 Hydrodynamic validation

272 The first step is the hydrodynamic validation. Since no measurements were performed on the
 273 study area, the model was validated against Acoustic Doppler Current Profiler (ADCP) and wave
 274 buoy using the LS2 configurations of CROCO and WW3. Sensitivity analysis was performed on
 275 the hydrodynamic changes occurring between LS2 and B1 area modelling (B1 boundary
 276 conditions are extracted from LS2) to find that no significant changes occurred and the validation
 277 at LS2 level is considered valid at B1 level.

278 The comparison of the simulated and measured currents was performed over its barotropic
 279 component. Figure 5 shows the comparison of the current magnitude and direction between 20
 280 May 2021 and 04 June 2021. The asymmetry between ebb and flood is well represented for the
 281 weak tidal conditions around 03 June while for the intense conditions in the middle of the
 282 comparison period, the model underestimates the flood peak. This could be attributed to the
 283 difference of bathymetry since LS2 configuration consider the HOMONIM bathymetry which
 284 has been surveyed in 2012. This difference stays however low with a RMSE = 0.16 m/s.
 285 Regarding the direction, the variation between ebb and flood is well represented with the
 286 direction varying between 75 and 265°N. The rapid turning of the tide at the beginning of each
 287 ebb/flood period is correctly represented despite some misrepresentation of short-term variations
 288 that sometimes occurs. It naturally increases the RMSE = 59.07° but the Willmott (1981) index
 289 shows that the representation stays correct with a value of 0.9.

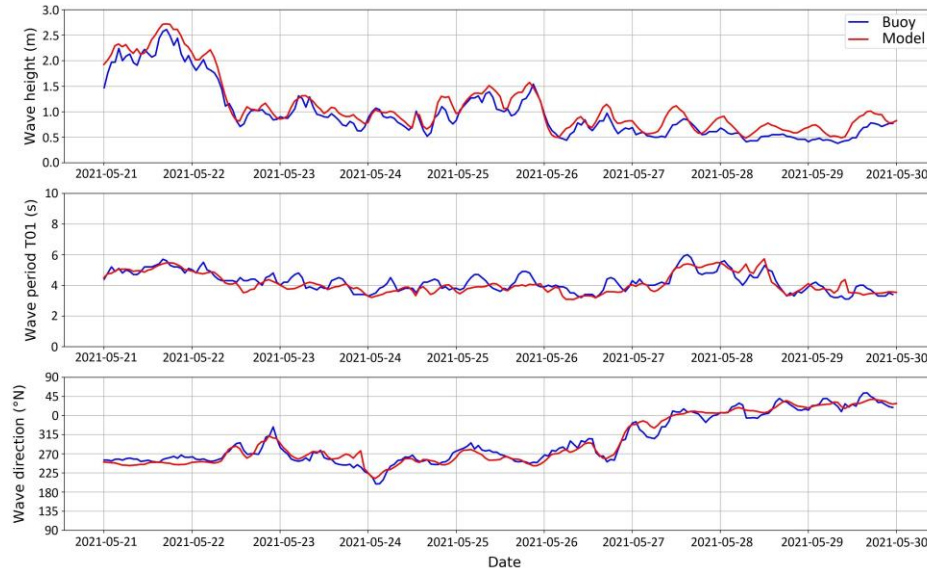
290



291
 292 **Figure 5. Current magnitude and direction comparison between model and ADCP**
 293 **measurements.**
 294

295 Regarding the waves, the following Figure 6 represents the comparison between model and
 296 observations between the 21 and the 30 May 2021. It shows an overall good accuracy of all
 297 components with correct statistics. The model accurately represents the variation of the
 298 significant wave height (RMSE = 0.16 m) which rises at the beginning of the period to reach
 299 almost 2.5 m on the first day and rapidly decreases to stay around 1 m for the following days.
 300 The wave period here does not show strong gradients and the model is in accordance with that
 301 with correct RMSE = 0.47. The RMSE value is however a boosted here by the fact that both
 302 model and buoy data do not actually show the same thing. The model returns current-corrected
 303 wave period, which is called the relative period, while we can see a clear variation due to the
 304 tidal current on the buoy data which returns the absolute wave period. This influence and the
 305 general discrepancy between model and measurements is however weak and the model is
 306 considered valid. To finish, the wave direction shows a very good match with even the rapid
 307 variations occurring on 26 May when the direction value drops from 315°N to 260°N within a
 308 couple of hours. Both RMSE = 18° and Willmott index of 0.96 demonstrates the good
 309 correlation of the model.

310



311
 312
 313 **Figure 6. Significant wave height, T01 period and mean wave direction comparison**
 314 **between WW3 simulation and the wave buoy.**

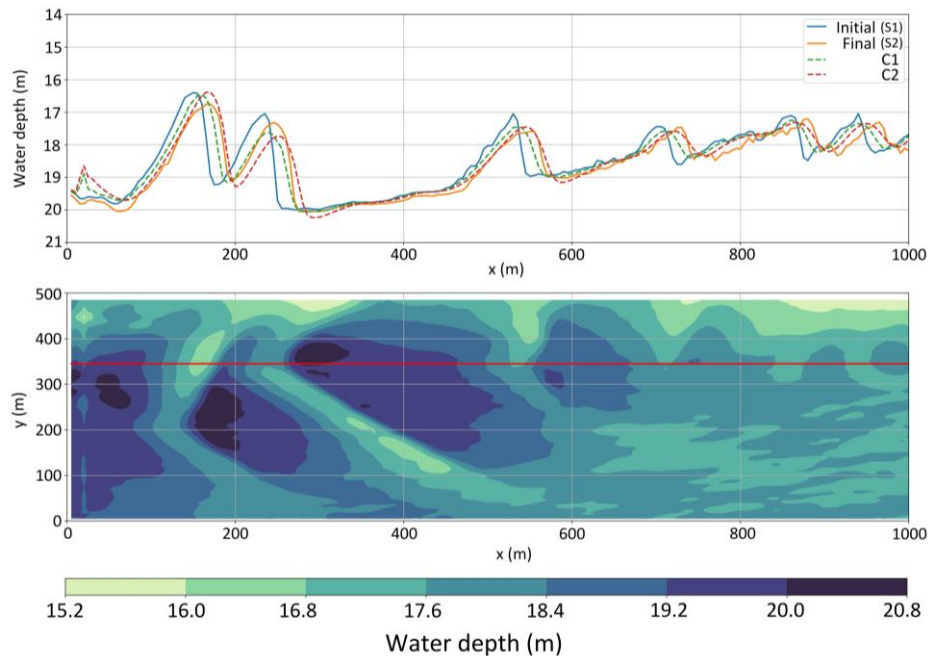
315 3.2 Comparison with observations along transects

316 A first analysis of the morphodynamic results was carried out along a transect extracted
 317 following a line perpendicular to the crestlines. However, since two barchans and a sinuous dune
 318 are present in the domain, several lines perpendicular to the crestlines can be defined. Therefore,
 319 the transect was extracted along the perpendicular of the three rectilinear dunes to catch all six
 320 dunes in a single row. On Figure 7, the longitudinal profile of the initial (S1) and final (S2)
 321 observations are compared to the modelling results of both C1 and C2 configurations. Observed
 322 data were submitted to the same low-pass filter to remove the secondary bedforms present
 323 throughout the study area. However, this filter is intentionally kept light and some secondary
 324 bedforms remain. To remove most of these small bedforms without changing the shape of the
 325 dune, the bathymetry is then smoothed a second time by applying a focal average. It considers a
 326 circle of 9 cells diameter (45 m considering the grid resolution) that slides along the domain and
 327 averages the center value by considering its neighbors. The observations are finally interpolated
 328 on the 5-m resolution modelling grid results to stay consistent with the model. Following the
 329 methodology of Nexer et al. (2023), the crests of all dunes are defined as the local minimum of
 330 water depth.

331 On this transect, difference between S1 and S2 shows that the crest height of the first three dunes
 332 (D1, D2 and D3) decrease in height by about 0.3 m. Furthermore, the vertical shape of the third
 333 dune is also modified with a rounder crest during the second survey than during the first. The
 334 three rectilinear dunes (D4, D5 and D6) do not show major changes in their crest height. They
 335 follow the general migration schema and migrate toward the east without significant changes.
 336 The model results generally follow the migration tendency revealed by the bathymetric surveys.
 337 The major difference between C1 and C2 configurations is the dune migration: migration rate is
 338 higher in C2 case and better matches the observation especially for the three rectilinear dunes
 339 than for C1. This result is in accordance with the roughness parameters which is 10 times higher
 340 for C2 than for C1. Regarding the crest height, both configurations show a similar pattern.
 341 Contrary to the observed morphodynamic, the model estimates an increase in the crest height of

342 D1 but underestimate it for D2 (difference of almost 0.7 m with S1 compared to a reduction of
 343 0.3 m in reality). The model accurately represents the variation of D3 and is consistent for both
 344 C1 and C2. For all dunes, C2 configuration is closer than C1 to the measured bathymetry with a
 345 better representation of the migration rate. This is confirmed by the Brier Skill Score ($BSS_{C1} =$
 346 0.75 and $BSS_{C2} = 0.87$). Following the classification proposed by Sutherland et al. (2004), both
 347 configurations can be considered as excellent. The model aims at correctly simulating dune
 348 dynamics, therefore the crest positions are important to consider the modelling as accurate. The
 349 Root Mean Square Error of the crest position for C1 and C2 are respectively $RMSE_{C1} = 9.35$ m
 350 and $RMSE_{C2} = 2.89$ m. On this transect, all dune crests have moved of about 20 m toward the
 351 east. This short movement combined with the low dune height explains the good BSS on both
 352 configurations. However, by comparing the RMSE on the crests positions, configurations C1 is
 353 accurate on the heights estimation but not on the crests positioning and therefore on the
 354 migration process. This is consistent with the results reported by Krabbendam et al. (2021) who
 355 have shown that the BSS should be considered carefully based on the results on 2D modelling
 356 along dunes.

357
 358



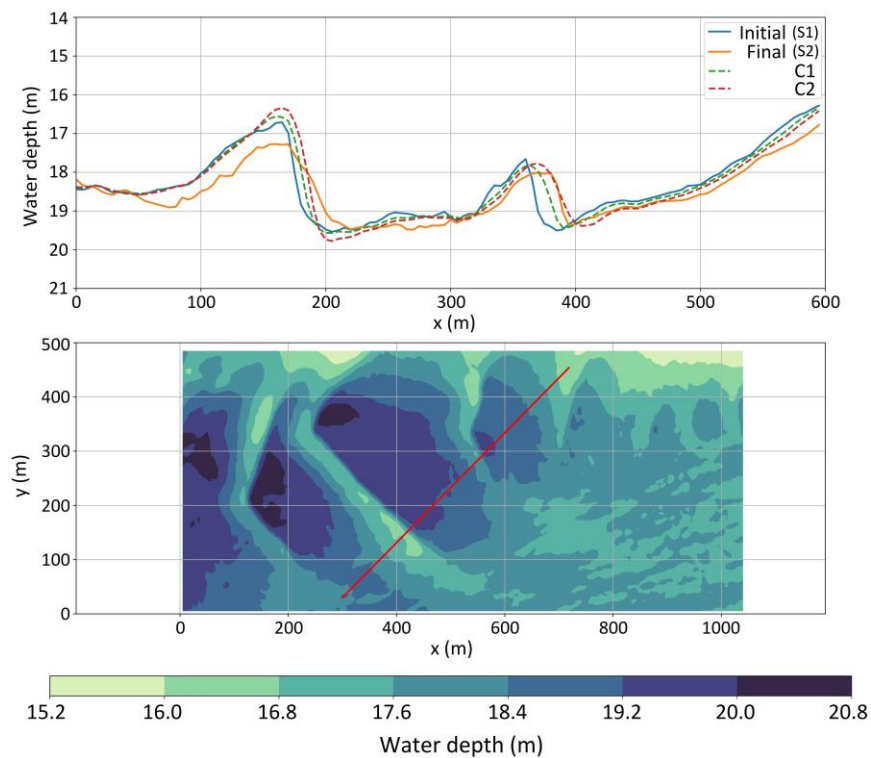
359
 360

361 **Figure 7. (top) Longitudinal profiles of the initial (S1) and final (S2) observations**
 362 **compared with C1 and C2 configurations results. (bottom) Synoptic view of the**
 363 **bathymetry estimated by C2 configuration. The red line represents the location of the**
 364 **transect.**

365

366 The validation using a single longitudinal profile and the comparison of crest position show that
 367 the C2 configuration performs better than C1 configuration. However, because of the presence of
 368 barchans and sinuous dunes, the comparison depends on the transect location. Following the
 369 same procedure, the bathymetric profile is extracted along a line perpendicular to the crest line of
 370 D2 crossing the area from South-East to North-West (Figure 8). Here the profile also catches the

371 third dune. Contrary to the previously analysed profile, both configurations do not model
 372 correctly the dynamic of dune D2. Difference between S1 and S2 shows that D2 migrates toward
 373 the east but experienced a large decrease of its crest height, which is not reproduced by the
 374 model. Here the crest height drop by about 0.7 m while C1 and C2 estimates an increase of
 375 respectively 0.1 and 0.3 m. Following these profiles, the estimations are not classified as
 376 excellent with BSS lower than 0.5 ($BSS_{C1} = 0.38$ and $BSS_{C2} = 0.45$). The RMSE should not be
 377 applied on only two crests positions. Therefore model and observation are only compared by the
 378 difference in meters. For both configurations, the position of D2 crest is well represented with a
 379 difference of 5 m only. However for D3, both C1 and C2 do not catch the strong movement
 380 occurring during the study period with respectively a difference of 15 and 10 m. By considering
 381 only the D2 dune, and this transect, the best model configuration is C1, which contradicts
 382 previous results.
 383



384
 385

386 **Figure 8. (top) Bathymetric transect of the initial and final observations compared with C1**
 387 **and C2 configurations results extracted along a line perpendicular to D2 crest line.**
 388 **(bottom) Synoptic view of the bathymetry estimated by C2 configuration. The red line**
 389 **represents the location of the transect.**

390 3.3 Comparison with observations over the area

391 To the authors knowledge, no validation was performed with a three-dimensional modelling of
 392 marine dunes against an observed bathymetry. Therefore, the validation process in this section is
 393 based on a classical procedure used to validate morphodynamic modelling of sand banks or
 394 coastlines (Sutherland et al., 2004 ; Ruggiero et al., 2009 ; Ranasinghe et al., 2011 ; Luijendijk et
 395 al., 2016). Following it, the BSS is estimated for both configurations considering the entire B1

396 domain. Results show that C2 better represents the dune migration with a $BSS_{C2} = 0.73$
 397 compared to C1 with a $BSS_{C1} = 0.56$. Here the BSS over the whole domain is lower than the
 398 BSS calculated using the longitudinal profile as it considers the error spotted on the southern part
 399 of D2 dune. Both configurations could however be considered as excellent which could be
 400 enough to validate the model. To identify the source of the error of both configurations, the
 401 Murphy-Epstein decomposition is applied and the results reported in the following Table 2. For
 402 both configurations the average bed level error γ and the normalization term ε are similar with a
 403 value of 0.04. Bottom roughness does not induce significant influence of these terms consistently
 404 with the results reported by Sutherland et al. (2004). A slight difference is estimated for the
 405 amplitude error with 0.07 for C1 and 0.002 for C2. These values are still close to zero which
 406 indicates an almost perfect modelling of the transported volume. The main source of error here
 407 comes from the phase (i.e. the position of the dunes), with $\alpha_{C1} = 0.65$ and $\alpha_{C2} = 0.75$.
 408

Variable name	α	β	γ	ε
C1	0.65	0.07	0.04	0.04
C2	0.75	0.002	0.04	0.04

409 **Table 2. Murphy-Epstein decomposition of the Brier Skill Score estimated for both C1 and**
 410 **C2 configuration over the entire B1 area.**

411
 412 To analyse this error, longitudinal transects are extracted every 5 m (the model resolution) and an
 413 average migration is estimated considering only the movement of the crests. All crests move as
 414 expected toward the east with average displacements ranging from 18.75 m for D5 to a
 415 maximum of 23.13 m for D4. The RMSE of crest positions are estimated for each dune
 416 independantly (Table 3). As a reminder, consistently with the model, observations were
 417 projected on a 5 m resolution grid. Therefore, the RMSE lower than 5 m calculated for C2 over
 418 dunes D1, D3, D4 and D6 and equal to 5 m for D5 clearly demonstrate that C2 configuration
 419 results can be considered as excellent. However, in the case of C1 configuration, bottom
 420 roughness is too low for the model to estimate a sufficient migration during the period. This lead
 421 to high difference of around 10 m for all dunes. Compared to the observed displacement of about
 422 20 m of each dune, this can be considered as a strong error and cannot be considered as a reliable
 423 comparison. This is in line with the previously described results which shows that C1
 424 configuration is not acceptable in term of crest positions. Both configurations show however
 425 strong RMSE for D2, with 16.6 and 14 m for C1 and C2, respectively. For C1 this demonstrates
 426 that the representation on all dunes have a lack of precision while it shows, for C2, a lack of
 427 precision on one dune only.
 428

429 **Table 3. Mean migrations and Root Mean Square Error (RMSE) of the crests position for**
 430 **each dune for both C1 and C2 configurations.**

Dune name	D1	D2	D3	D4	D5	D6
Mean migration (in m)	19.17	20.93	20.7	23.13	18.75	22.11
RMSE C1	10.38	16.6	11.51	12.78	10.75	11.81
RMSE C2	5.31	14	4.38	3.19	5	2.56

432

433 Here the results show that the use of the BSS over the whole area does not seem adapted for this
434 kind of modelling. The validation process needs to be improved with an analysis of each dune
435 position. However, in the current case, the combined BSS with the analysis of the crest position
436 is easy to perform because of the small number of dunes but, in the case of the presence of
437 dozens of dunes, this analysis is too labourious to be used. This procedure should then be
438 improved in order to evaluate the height and crest positions in a reliable way.

439 3.4 Three-dimensional validation

440 In this section, a validation method of a three-dimensional dune migration modelling is
441 proposed. It is based on two main dimensions. The vertical dimension with the estimation of the
442 depths and dune heights and the horizontal dimension with the position of the crests and troughs
443 of each dune.

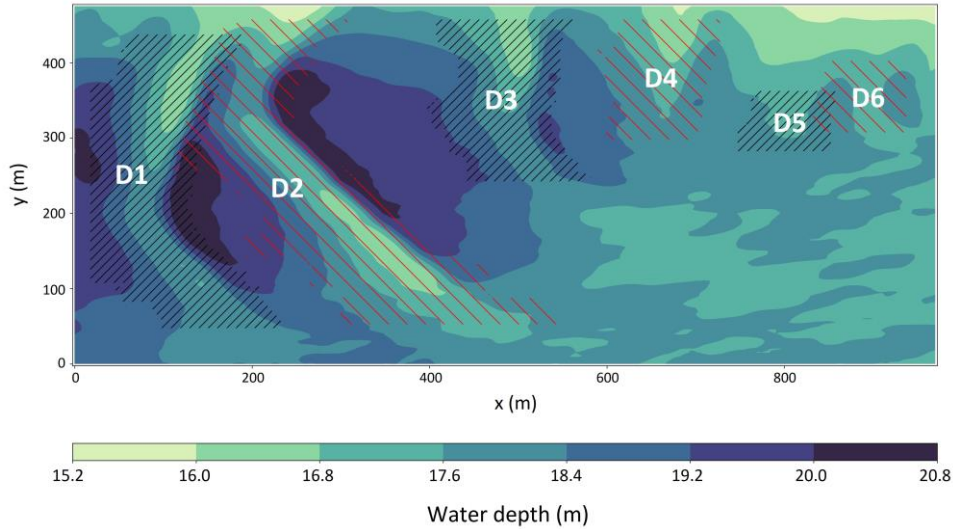
444 *Vertical validation*

445
446 As described earlier, the vertical validation over an area is made by the calculation of the Brier
447 Skill Score (BSS) which considers the entire B1 domain. However, contrary to the modelling of
448 a sand bank or a coastline, here the focus is made on the modelling of marine dunes which
449 represent only a small part of the actual domain. In fact, another particularity of the B1 domain,
450 is that it is composed by large plain areas where only secondary dunes are present. The model
451 does not consider these shapes, as they are below the resolution required and not the focus of the
452 present study, and smoothed the bathymetry leading to a global error. Including these plain areas
453 in the validation process means that the dune migration validation depends on the correct
454 modelling of areas that are not related to the very large dunes. To overcome this issue, it is
455 necessary to consider only the dune areas. This requires to accurately identify both crests and
456 troughs. In the preliminary analysis (Nexer et al, 2023), the crests were considered as the local
457 minima of water depths. Consistently, the troughs were identified as the local maxima of water
458 depths. However, in the marine environment, through identification is complex and they are
459 either considered as the foot of the stoss or lee slope (Duffy, 2012) or the point where the
460 maximum value of the curvature is estimated (Van Dijk et al., 2012; Lebrec et al., 2022). Duffy
461 (2012) considers using the foot of the stoss or lee slope for a solitary bedform while here
462 multiple dunes are present. The definition based on the calculation of the curvature seems then to
463 be adapted for the current case and the methodology described by Lebrec et al. (2022) is applied
464 over the B1 domain.

465
466 All longitudinal profiles were extracted every 5 m along the y-axis for both observations and
467 model results. Despite the low-pass filter, some remaining secondary bedforms could induce
468 multiple crests detection. The point with the minimum water depth is then considered as the
469 crests of each dunes. The curvature is calculated as the second derivative of the bathymetric
470 profile. The first local maximum of curvature on each side of the crests positions is considered as
471 the eastern and western troughs of the dune.

472 Considering the eastern migration pattern, the area occupied by each dunes is taken as starting on
473 the west with the western trough of the initial observation and, on the east, with the eastern
474 trough of the final observation. The 6 dunes areas are then identified as shown on Figure 9. To
475 avoid any boundary issues, the model and observations data do not account for the first 50 m
476 along to the boundaries. This limits the identification of the western trough of D1 which will not
477 be accounted into the comparison process. The identified areas show that dunes D1 and D2

478 follow each other on their northern part while there is a large plain area that separates them on
 479 the southern part. The same thing is observed for D5 which northern part sticks with the southern
 480 part of D6. The other dunes D3 and D4 are isolated with plain areas that separates them from the
 481 others.
 482



483
 484 **Figure 9. Area of the six dunes over the B1 domain. The colormap represents the**
 485 **bathymetry estimated by configuration C2.**
 486

487 Using this identification, the Brier Skill Score is applied on the six areas for both configurations.
 488 This allows to assess the capability of the model to simulate the area where there is a dune
 489 movement. As described earlier, it also discards the large plain on the south-east, which
 490 represents almost 1/4th of the model domain, and also other part which are not related to the
 491 dunes. For C1 and C2 the BSS is respectively of 0.62 and 0.81. Here the difference with the BSS
 492 estimated by considering the entire B1 area ($BSS_{C1} = 0.56$; $BSS_{C2} = 0.73$) shows that C2 was
 493 slightly more penalized by the plain areas in the estimation of its accuracy. This could be
 494 explained by the fact that C2 has less error over the dune than C1. The error on the plains areas
 495 on the south-east could then become more important in the entire calculation which would then
 496 reduce the skill score.

497 The BSS can also be applied over each dune separately. The results show that for both
 498 configurations, D2 is the least well represented with a $BSS_{C1-D2} = 0.51$ and $BSS_{C2-D2} = 0.68$
 499 (Table 4). The scores for C1 configuration are quite similar for all the other dunes except D1
 500 while for C2 there are larger differences between D2 and all other dune that show $BSS \geq 0.8$. It
 501 highlights the fact that the model does not catch all changes in D2.
 502

503 **Table 4. Brier Skill Score (BSS) estimated for each dune areas for C1 and C2**
 504 **configurations.**

Dune name	D1	D2	D3	D4	D5	D6
C1	0.74	0.51	0.68	0.62	0.62	0.52
C2	0.9	0.68	0.92	0.88	0.83	0.8

505
 506 *Horizontal validation*
 507

508 The crest and trough positions are compared for both configurations with the new identification
 509 methodology. The RMSE of the crest and trough positions is estimated for all dunes together
 510 except for the western trough for which the dune D1 is not considered as its location is limited by
 511 the area boundaries. These results first highlight strong differences of the trough locations with
 512 the observations for both configurations. The western troughs are the least well represented for
 513 C1 and C2 with RMSE of respectively 21.84 and 17.89 m while on the eastern troughs the
 514 RMSE is better with respectively 17.74 and 12.84 m. This highlights that even using the
 515 identification process described by Lebrec et al. (2022), the location of the troughs in a marine
 516 environment cannot be accurate enough for this kind of comparison. For long term simulations
 517 like the present study, the crests positions seems then to be the better choice for the migration
 518 validation.

519

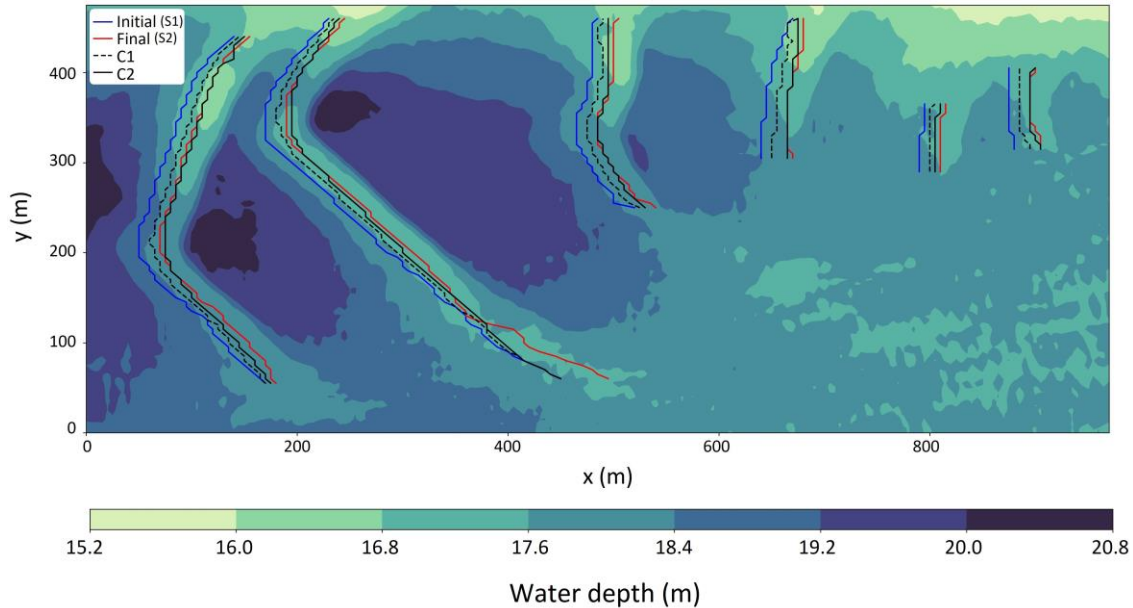
520 **Table 5. Root Mean Square Error (RMSE) estimated for western and eastern troughs and**
 521 **crest positions for both C1 and C2 configurations.**

Variable name	Western troughs	Crests	Eastern troughs
C1	21.84	13.1	17.74
C2	17.89	8.57	12.84

522

523 In the present study, the crest locations RMSE demonstrate the difference between
 524 configurations with for C1 and C2 values of respectively 13.1 m and 8.57 m. The error estimated
 525 with C2 configuration is not far from the model resolution (5 m) but cannot be considered as
 526 excellent. Following the mathematical definition of the Root Mean Square Error, this statistics
 527 would give more weight to the strong errors. This means that if the crest position is not
 528 accurately modelled on a small part of the dune, this would increase the RMSE. Figure 10 shows
 529 the crest locations for initial and final observations and for C1 and C2 configurations. It
 530 highlights that globally the crests position estimated by C2 configuration is close to the reference
 531 while C1 estimations are almost entirely “half way” between initial and final observations. In the
 532 case of C2, the crests positions even overlapped with the reference on the major part of D3, D4
 533 and D6. However, the crest position during the second bathymetric survey shows that the D2 has
 534 moved from its initial position by about 40 m on its southern horn. Both configurations did not
 535 represent this movement and the RMSE is then naturally increased by it. A second limitation of
 536 the RMSE here, is also that it does not consider the crests initial position and it could be difficult
 537 to assess the precision of a model.

538



539
540
541 **Figure 10. Locations of dunes' crests of initial and final observations compared with**
542 **predictions of C1 and C2 configurations. The colormap represent the bathymetry**
543 **estimated by C2 configuration.**
544

545 Sutherland et al. (2004) have described that a statistic should be transferable from a dataset to
546 another. Therefore, the use of the Brier Skill Score might be a good option to include the initial
547 crest positions and allow to estimate the model accuracy. The proposition made here is then to
548 estimate the BSS by considering all positions of crests as the dataset. For both C1 and C2 the
549 estimated value is respectively $BSS_{C1} = 0.62$ and $BSS_{C2} = 0.84$. Here the difference estimated
550 between the configurations is of the same order as the difference estimated for the vertical
551 comparison. However, the classification proposed by Sutherland et al. (2004) might not be
552 adapted here and these scores should not be considered the same way. Indeed, as described
553 before, C1 crest position is almost entirely “half way” between initial and final observations. The
554 score of 0.62 is thus logical. An “excellent” modelling of the crests position should so be
555 considered for scores greater or equal to 0.8 which, as described by C2 configuration results,
556 induce an accurate representation of the crests positions.
557

558 Using this methodology, both vertical and horizontal dimension show a good skill score for the
559 C2 configuration. On the contrary, C1 is accurate on the vertical dimension but does not
560 represent well the crests' positions. The C2 configuration is therefore considered as valid here
561 while C1 is not.
562

563 4. Discussion

564 4.1 Two and three dimensions

565 Among the different morphodynamic studies, most of them use a two-dimensional vertical
566 model (2DV) (Nemeth et al., 2007 ; Tonnon et al., 2007 ; Krabbendam et al., 2021). In these
567 studies, the dune field is composed by rectilinear dunes. The use of a 2D validation process

568 based on transect comparison is so well fitted. This is however not the case for some 3D
569 morphodynamic models. Indeed, as shown by the results of the 2D analysis, the barchan dune D2
570 has a faster crest displacement on its toe in the north than on its horn in the south (nomenclature
571 based on Couldrey et al., 2019). This is in line with the results of Charru and Laval (2013), who
572 have reported a reduction of the current intensity over the horns of a barchan. The model is so
573 able to reproduce this migration on its northern part but fails on its southern part with almost no
574 displacement of the crest (Figures 7 and 8). This demonstrates the need to prioritize a validation
575 over the area or at least over multiple transects to avoid missing such errors that could occurs
576 over small areas.

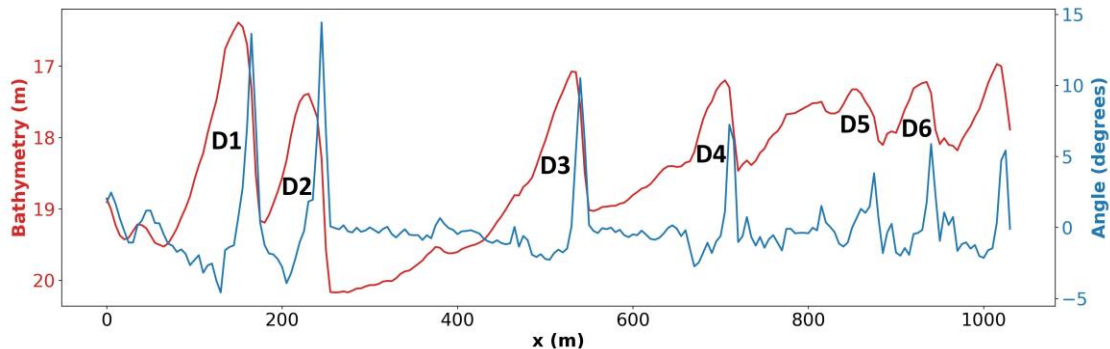
577 The 3D validation method also has the advantage to better assess the difference between
578 configurations. Over the first transect (Figure 7), the difference between C1 and C2 BSS is 0.12
579 ($BSS_{C1} = 0.75$; $BSS_{C2} = 0.87$) while over the second transect it is equal to 0.07 ($BSS_{C1} = 0.38$;
580 $BSS_{C2} = 0.45$). Both configurations could then be considered equivalent in term of validity. On
581 the contrary, the difference between the skill scores considering the B1 area is 0.17 ($BSS_{C1} =$
582 0.56 ; $BSS_{C2} = 0.73$). A value that is even increased to 0.19 when considering the dunes' areas
583 ($BSS_{C1} = 0.62$; $BSS_{C2} = 0.81$). Therefore, a 3D comparison accentuates the differences between
584 the configurations and allows a better assessment of numerical modelling results. A 3D
585 validation process might then need to be considered on an area even if the dunes are rectilinear.
586 This could bring more insight about the configurations reliability than a 2D analysis and improve
587 the validation process itself.

588 4.2 Limitations and advantages of the proposed method

589 The previous results demonstrate that the use of a 3D model with a 3D validation method is
590 necessary in the current case. However, regarding the vertical dimension, the method used for
591 coastlines or sand banks does not seems adapted to marine dune migration modelling. By
592 considering the entire domain for the BSS calculation, the large plains in the southeastern part of
593 the domain would be included. This implies that the validation of the dunes' migration modelling
594 depends on the correct modelling of secondary bedforms located hundreds of meters away from
595 the primary dunes. Here, the model does not consider these bedforms and smooths the entire
596 southeastern area of the B1 domain. This leads to a source of error which reduces the BSS. The
597 proposed method considers to avoid these plains to focus on the areas where the dunes migrate.
598 The identification of these areas is however a limitation of the method. The comparison made on
599 the trough and crest positions shows strong errors on the trough positions compared to the crests.
600 This error could be attributed to a difficult identification of the troughs. Indeed, as described by
601 Lefebvre et al. (2021), in an environment dominated by tidal current, bedforms have steeper
602 slopes close to the crest, and flat troughs. This is confirmed here by the filtered profiles shown
603 on Figure 11. The slope is calculated on the same longitudinal profile displayed on Figure 7 for
604 the initial observation. The maximum angle is found on the upper part of the lee side, closer to
605 the crest than to the eastern trough with angles reaching a maximum of 14° for D2. Regarding
606 the horizontal position, the maximum slope of dune D4 is also closer to the crest while for the
607 others it is located on the middle part of the lee side. This facilitates the identification of the
608 crests but it is quite difficult to identify the troughs. The dune areas identified here using the
609 methodology defined by Lebrec et al. (2022) is limited as their boundaries are defined by the
610 western and eastern troughs. Moreover, this also induce that the method should be adapted to the
611 environment. In the marine environment, the crests positions are easily identified and then the
612 comparison of their position with the observations make sense. In rivers however, Cisneros et al

613 (2020) have reported that dunes have a relatively flat crest and maximum slope over their lower
 614 lee side. The method might need to be applied on the troughs positions in the river environment
 615 to consider this difference.

616



617

618

619 **Figure 11. (Red) Longitudinal profiles of the initial observations extracted along the**
 620 **transect represented on Figure 7. (Blue) Slope on the bathymetry. The calculation is based**
 621 **on the bathymetric profile represented by the blue line.**

622

623 The comparison of the crest (or trough) position is mostly performed using the RMSE in 2DV
 624 models. However, in a three-dimensional validation that considers all crests positions, this leads
 625 to two issues that should be considered. First, in the present study, the major source of error on
 626 both configurations comes from the southern part of dune D2. Observations show a large
 627 displacement of the crests of about 30-40 m while both configurations do not estimate any
 628 movement. This explain the RMSE that is high even for C2 (Table 2) which is considered as
 629 valid. However, when it comes to the modelling of the morphodynamic of an area, even for a
 630 sand bank or other cases, the validation process should focus on knowing if the model is globally
 631 accurate. Here if the RMSE is applied on all crest positions, it would be increased by this error
 632 occuring on a small part of one dune. The entire simulation would then be penalized. Other
 633 metrics could have been used such as the Mean Average Error (MAE) or the Mean Square Error
 634 (MSE), however same as the RMSE all these metrics do not account for the initial crest position.
 635 This lead then to the second issue, which is that the modelling it made to represent the migration
 636 of the dune and not the crest positions. Using the BSS puts the error in context. This leads
 637 however to another limitation of the proposed method. All dunes migrate following the eastern
 638 direction. Here it allows an easy comparison of the crest positions with only a difference in the
 639 longitudinal direction. However, over a larger domain, multiple dune migration direction could
 640 be present. The method should then be adapted to the domain by comparing the dune migration
 641 in the correct direction.

642 5 Conclusions

643 In the context of the numerical modelling of a dune field, the question of the validation of a
 644 three-dimensional model was addressed. This was studied with validation methods based on the
 645 comparison with bathymetric survey using either a transect or the entire area to assess the model
 646 reliability. The main outcomes of the study are as follows :

647

648 1. The application of the Brier Skill Score on the entire domain does not seem to be adapted to
 649 validate a morphodynamic model focusing on marine dune migration. In this case the
 650 southeastern part of the domain is composed by a large plain area which is irrelevant to assess
 651 the model reliability. The method proposed here is then to only consider the dunes' areas to
 652 estimate this score and avoid considering irrelevant areas in the validation process.

653
 654 2. In the same context, the calculation of the RMSE of the crest positions does not seem to be
 655 adapted here to the validation process. This score will be boosted by a strong difference occurring
 656 on a small part of a dune. Therefore, to overcome this issue, the proposed method considers the
 657 application of the Brier Skill Score by considering the crest positions as the dataset. The error is
 658 then put in context and allows to better assess the model capability.

659
 660 The findings of this study do not have the intention to question the validity of other models and
 661 more studies using this method needs to be performed to assess its reliability. The modelling of a
 662 marine dune field is quite new and the method that is described here is then a proposal to see the
 663 validation of this kind of model in another way.

664 **Acknowledgments**

665 This work is part of the MODULES project which receives funding from France Energies
 666 Marines and its members and partners, as well as French State funding managed by the French
 667 National Research Agency under the France 2030 Investment Plan (ANR-10-IEED-0006-34).

668 **References**

670 Auclair, F., Benschila, R., Bordoio, L., Boutet, M., Brémond, M., Caillaud, M., Cambon, G.,
 671 Capet, X., Debreu, L., Ducouso, N., Dufois, F., Dumas, F., Ethé, C., Gula, J., Hourdin, C., Illig,
 672 S., Jullien, S., Le Corre, M., Le Gac, S., et al. (2022), Coastal and Regional Ocean COMMUNITY
 673 model (1.3). <https://doi.org/10.5281/zenodo.7415343>

674
 675 Barrie, J.V., Conway, K.W. (2014), Seabed characterization for the development of marine
 676 renewable energy on the Pacific margin of Canada. *Continental Shelf Research*, 83, 45-52.
 677 <https://doi.org/10.1016/j.csr.2013.10.016>

678
 679 Belderson, R.H., Johnson, M.A., Kenyon, N.H. (1982), Bedforms. *Offshore Tidal Sands,
 680 Processes and Deposits*, Chapman and Hall. <https://doi.org/10.1007/978-94-009-5726-8>.

681
 682 Bennet, W.G., Karunarathna, H., Reeve, D.E., Mori, N. (2019), Computational modelling of
 683 morphodynamic response of a macro-tidal beach to future climate variabilities. *Marine Geology*,
 684 415. <https://doi.org/10.1016/j.margeo.2019.105960>.

685
 686 Blaas, M., Dong, C., Marchesiello, P., McWilliams, J.C., Stolzenbach, K.D. (2007), Sediment-
 687 transport modeling on southern Californian shelves: A ROMS case study. *Continental shelf
 688 research*, 27, 832-853. <https://doi.org/10.1016/j.csr.2006.12.003>.

689
 690 Blondeaux, P., Vittori, G. (2016), A model to predict the migration of sand waves in shallow
 691 tidal seas. *Continental Shelf Research*, 112, 31-45. <https://doi.org/10.1016/j.csr.2015.11.011>.

692

693 Bonnefille, R., Lepetit, J.-P., , Graff, M., Leroy, J. (1971), Nouvel avant-port de Dunkerque,
694 Mesure en nature. *Laboratoire National d'Hydraulique, Report HC042/05.*

695

696 Charru, F., Laval, V. (2013), Sand transport over a barchan dune. *MARID IV – 15 & 16 April*
697 *2013- Bruges, Belgium.*

698

699 Cisneros, J., Best, J., van Dijk, T., Paes de Almeida, R., Amsler, M., Boldt, J., Freitas, B.,
700 Galeazzi, C., Huizinga, R., Ianniruberto, M., Ma, H., Nittrouer, J.A., Oberg, K., Orfeo, O.,
701 Parsons, D., Szupiany, R., Wang, P., Zhang, Y. (2020), Dunes in the world's big rivers are
702 characterized by low-angle lee-side slopes and a complex shape. *Nature Geoscience, 13*, 156-
703 162. DOI : 10.1038/s41561-019-0511-7.

704

705 Couldrey, A., Knaapen, M., Marten, K., Whitehouse, R. (2019), Barchan vs Monopile : what
706 happens when a barchan dune finds an obstacle in its path ?. *Marine and River Dune Dynamics –*
707 *MARID VI*, 1-3 April 2019, Bremer, Germany.

708

709 Dam, G., van der Wegen, M., Labeur, R.J., Roelvink, D. (2016), Modeling centuries of estuarine
710 morphodynamics in the Western Scheldt estuary. *Geophysical Research Letters, 43*, 3839-3847.
711 doi:10.1002/2015GL066725.

712

713 Damen, J.M., van Dijk, T.A.G.P., Hulscher, S.J.M.H. (2018), Spatially varying environmental
714 properties controlling observed sand wave morphology. *Journal of Geophysical Research: Earth*
715 *Surface, 123*(2), 262-280. doi:10.1002/2017JF004322

716

717 van Dijk, T.A.G.P., van Dalfsen, J.A., Van Lancker, V., van Overmeeren, R.A., van Heteren, S.,
718 Doornenbal, P.J. (2012), Benthic Habitat Variations over Tidal Ridges, North Sea, the
719 Netherlands. *Seafloor Geomorphology as Benthic Habitat, 241–249.*
720 <https://doi.org/10.1016/B978-0-12-385140-6.00013-X>

721

722 Doré, A., Bonneton, P., Marieu, V., Garlan, T. (2018), Observation and numerical modeling of
723 tidal dune dynamics. *Ocean dynamics, 68*, 589-602. <https://doi.org/10.1007/s10236-018-1141-0>.

724

725 Duffy, G. (2012), Patterns of morphometric parameters in a large bedform field: Developpement
726 and application of a tool for automated bedform morphometry. *Irish Journal of Earth Sciences,*
727 *30*, 31-39. doi.10.3318/IJES.2012.30.31.

728

729 Ernsten, V.B., Noormets, R., Winter, C., Bartholomä, A., Flemming, B.W., Bartholdy, J. (2004),
730 Development of subaqueous barchan dunes due to lateral grain size variability. *MARID,*
731 *Enschede Netherlands*, p.8.

732

733 Knaapen, M.A.F., Hulscher, S.J.M.H., Vriend, H.J., Stolk, A. (2001), A new type of sea bed
734 waves. *Geophysical Research Letters, 28*, 1323-1326. <https://doi.org/10.1029/2000GL012007>.

735

- 736 Krabbendam, J., Nnafie, A., de Swart, H., Borsje, B., Perk, L. (2021), Modelling the past and
737 future evolution of tidal sand waves. *Journal of marine science and engineering*, 9, 1071.
738 <https://doi.org/10.3390/jmse9101071>.
739
- 740 Le Bot, S., Trentesaux, A. (2004), Types of internal structure and external morphology of
741 submarine dunes under the influence of tide- and wind-driven processes (Dover Strait, northern
742 France). *Marine Geology*, 211, 143-168. <https://doi.org/10.1016/j.margeo.2004.07.002>.
743
- 744 Lebrec, U., Riera, R., Paumard, V., O'Leary, M.J., Lang, S.C. (2022), Automatic Mapping and
745 Characterisation of Linear Depositional Bedforms: Theory and Application Using Bathymetry
746 from the NorthWest Shelf of Australia. *Remote Sensing*, 14, 280. DOI : 10.3390/rs14020280.
747
- 748 Lefebvre, A., Herrling, G., Becker, M., Zorndt, A., Krämer, K., Winter, C. (2021), Morphology
749 of estuarine bedforms, Weser Estuary, Germany. *Earth Surface Processes and Landforms*, 1-
750 15. <https://doi.org/10.1002/esp.5243>.
751
- 752 Luijendijk, A.P., Ranasinghe, R., de Schipper, M.A., Huisman, B.A., Swinkels, C.M., Walstra,
753 D.J.R., Stive, J.F. (2017), The initial morphological response of the Sand Engine: A process-
754 based modelling study. *Coastal engineering*, 119, 1-14.
755 <http://dx.doi.org/10.1016/j.coastaleng.2016.09.005>.
756
- 757 Németh, A.A., Hulscher, S.J.M.H., Van Damme, R.M.J. (2007), Modelling offshore sand wave
758 evolution. *Continental Shelf Research*, 29, 713-728. <https://doi.org/10.1016/j.csr.2006.11.010>.
759
- 760 Nexer, M., Bacha, M., Bary, M., Gangloff, A., Robert, A., Amara, R., Blanpain, O., Parent, B.,
761 Desroy, N., Garlan, T., Le Bot, S., Michelet, N., Quillien, N. (2023), Les dunes sous-marines et
762 leur écosystème sous contraintes anthropiques. Recommendation report of the DUNES project,
763 France Energies Marines.
764
- 765 Ranasinghe, R., Swinkels, C.M., Luijendijk, A.P., Roelvink, J.A., Bosboom, J., Stive, M.J.F.,
766 Walstra, D.J.R. (2011), Morphodynamic upscaling with the MORPHAC approach: dependencies
767 and sensitivities. *Coastal Engineering*, 58. <https://doi.org/10.1016/j.coastaleng.2011.03.010>
768
- 769 Ruggiero, P., Walstra, D.J.R., Gelfenbaum, G., Van Ormondt, M. (2009), Seasonal-scale
770 nearshore morphological evolution: Field observations and numerical modeling. *Coastal*
771 *Engineering*, 56, 1153-1172. doi:10.1016/j.coastaleng.2009.08.003.
772
- 773 Sutherland, J., Peet, A.H., Soulsby, R.L. (2004), Evaluating the performance of morphological
774 models. *Coastal engineering*, 51, 917-939. <https://doi.org/10.1016/j.coastaleng.2004.07.015>.
775
- 776 Scott, T.R., Mason, D.C. (2007), Data assimilation for a coastal area morphodynamic model:
777 Morecambe Bay. *Coastal engineering*, 54, 91-109.
778 <https://doi.org/10.1016/j.coastaleng.2006.08.008>.
779

- 780 Tonnon, P.K., van Rijn, L.C., Walstra, D.J.R. (2007), The morphodynamic modelling of tidal
781 sand waves on the shoreface. *Coastal engineering*, 54, 279-296.
782 <https://doi.org/10.1016/j.coastaleng.2006.08.005>.
783
- 784 Van den Berg, J., Sterlini, F., Hulscher, S.J.M.H., van Damme, R. (2012), Non-linear process
785 based modelling of offshore sand waves. *Continental shelf research*, 37, 26-35.
786 <https://doi.org/10.1016/j.csr.2012.01.012>.
787
- 788 Warner, J. C., Sherwood, C. R., Signell, R. P., Harris, C. K., and Arango, H. G. (2008),
789 Development of a three-dimensional, regional, coupled wave, current, and sediment-transport
790 model. *Computers & Geosciences*, 34(10), 1284–1306.
791 <https://doi.org/10.1016/j.cageo.2008.02.012>.
792
- 793 Whitehouse, R.J.S., Damgaard, J.S., Langhorne, N. (2000), Sandwaves and seabed engineering:
794 the application to submarine cables. *Proceeding of Marine Sandwaves Dynamics*, MARID, 227-
795 234.
796
- 797 Willmott, C. (1981), On the validation of models. *Phys. Geogr.*, 2, 184–194.
798 <https://doi.org/10.1080/02723646.1981.10642213>
799
- 800 Wu, W., Lin, Q. (2014), Nonuniform sediment transport under non-breaking waves and currents.
801 *Coastal Engineering*, 90, 1-11. <http://dx.doi.org/10.1016/j.coastaleng.2014.04.006>.